Correlation between present-day model simulation of Arctic cloud radiative forcing and sea ice consistent with positive winter convective cloud feedback

Correlation between present-day model simulation of Arctic cloud radiative forcing and sea ice consistent with positive winter convective cloud feedback

Benjamin D. Leibowicz,[1] Dorian S. Abbot,[2] Kerry Emanuel,[3] and Eli Tziperman[1,4]

Received 25 January 2012; revised 7 May 2012; accepted 11 June 2012; published 20 July 2012.

[1] A positive feedback on winter sea-ice loss, based on warming due to radiative forcing caused by the onset of convective clouds in response to sea-ice loss, has recently been proposed. This feedback has thus far been investigated using a hierarchy of climate models in high CO_2 scenarios. This paper examines the possibility that such feedback may be active within present-day like Arctic variability, using model output from two reanalysis models. It is emphasized that Arctic surface fluxes, radiative fluxes and clouds are effectively unconstrained by observations in reanalysis products. Consequently, the results here should be viewed only as a model study of the feedback in present-day model climate variability. Model winter sea ice and cloud radiative forcing are found to co-vary strongly and locally, consistent with a strong convective cloud feedback, which may contribute to sea ice variability. Furthermore, the anti-correlation between the two variables is found to be as strong in the model output analyzed here as in the IPCC global climate models that simulate the convective cloud feedback most strongly at high CO_2. In those IPCC models the convective cloud feedback contributes to a total loss of winter sea ice in a CO_2 quadrupling scenario. These results do not necessarily prove that this feedback exists in the present-day Arctic and demonstrating this will require further study using actual Arctic observations.

Citation: Leibowicz, B. D., D. S. Abbot, K. Emanuel, and E. Tziperman (2012), Correlation between present-day model simulation of Arctic cloud radiative forcing and sea ice consistent with positive winter convective cloud feedback, *J. Adv. Model. Earth Syst., 4*, M07002, doi:10.1029/2012MS000153.

1. Introduction

[2] The coupled global climate models used for the Intergovernmental Panel on Climate Change (IPCC) assessment produce forecasts of wintertime sea ice at $CO_2=1120$ ppm that span the entire possible range, with some models predicting very little change in wintertime sea-ice extent and others predicting complete loss of winter sea ice in the Arctic [*Winton*, 2006]. Given the importance of Arctic sea ice for Arctic ecosystems [*Smetacek and Nicol*, 2005; *McBean et al.*, 2005], and the potentially large economic impact that loss of Arctic sea ice could have due to expanded shipping routes and increased recovery of natural resources, it is important to identify the reasons for this spread in forecasts and attempt to narrow it.

[3] Clouds strongly influence the radiation balance in the Arctic [e.g., *Curry and Ebert*, 1992] by both reflecting incoming solar radiation and reducing emission of infrared radiation to space. In the summer, cloud reflection of solar radiation dominates and clouds tend to cool the surface in the Arctic [*Liu et al.*, 2008]. In the winter, when solar radiation is low, clouds tend to warm the surface [*Liu et al.*, 2008]. Given the large effect clouds can have on surface climate, one would expect that they may also play an important role in sea-ice variability.

[4] *Abbot and Tziperman* [2008a] proposed a positive wintertime feedback between convective clouds and sea-ice loss. *Abbot et al.* [2009b] showed that the differing activity of this feedback in different global climate models helps explain some of the large discrepancies between model sea-ice forecasts. This feedback is initiated by CO_2-induced warming, which causes initial sea-ice loss, allowing increased heat and moisture fluxes from the ocean surface to the atmosphere. This destabilizes the atmosphere, causing atmospheric convection, which produces optically-thick tropospheric convective clouds and enhanced moisture. These clouds and moisture trap

[1]Department of Earth and Planetary Sciences, Harvard University, Cambridge, Massachusetts, USA.
[2]Department of Geophysical Sciences, University of Chicago, Chicago, Illinois, USA.
[3]Program in Atmospheres, Oceans, and Climate, Massachusetts Institute of Technology, Cambridge, Massachusetts, USA.
[4]School of Engineering and Applied Sciences, Harvard University, Cambridge, Massachusetts, USA.

1942-2466/12/2012MS000153

outgoing longwave radiation and therefore result in further warming and further sea-ice loss. Because of the destabilizing effect of the strong radiative cooling on the wintertime Arctic atmosphere, this feedback is most active during winter in models [*Abbot and Tziperman*, 2008b; *Abbot et al.*, 2009a], when solar radiation and shortwave cloud radiative forcing are small.

[5] Although this convective cloud feedback is active to some degree in all of the IPCC models applied to a scenario in which CO_2 is quadrupled [*Abbot et al.*, 2009b], the strength of the feedback and the CO_2 concentration at which it activates differ among these models. It is therefore of interest to analyze this feedback in additional settings and study its strength and robustness.

[6] Observations do support an increase in convection and convective clouds associated with a decrease in sea ice during fall [*Schweiger et al.*, 2008; *Kay and Gettelman*, 2009], but the magnitude of a potential feedback has not been constrained and its wintertime activity has so far not been considered. Furthermore, cloud rolls have been observed near the ice edge in the Bering sea [e.g., *Walter*, 1980], as well as the development of convection cells in the flow of air from over sea ice to over open water [*Brummer*, 1997]. Open leads in winter can result in plumes that seem to develop via atmospheric convection and reach large vertical and horizontal distances [*Schnell et al.*, 1989; *Pinto et al.*, 1995] and potentially affect radiative balance this way. Model studies also found that Arctic winter sea-ice leads can result in convective plumes and in a significant increase in downwelling long wave radiation at the surface, and noted the similarity of such results to some observations of the Surface Heat Budget of the Arctic Ocean project (SHEBA) [*Zulauf and Krueger*, 2003a, 2003b].

[7] It has been known for a while that sea-ice loss is correlated with increased cloud fraction [e.g., *Palm et al.*, 2010], as well as that this significantly affects radiative balance and can lead to significant surface warming through most of the year [e.g., *Shupe and Intrieri*, 2004]. Such observations are consistent with parts of the convective cloud feedback loop, although cannot be seen as a verification and quantification of the complete feedback loop (coincidentally, convection is not discussed in these two specific papers).

[8] The role of clouds in Arctic climate has been studied extensively by both individual researchers and in collaborative field campaigns, including in the Coordinated Eastern Arctic Experiment (CEAREX) [e.g., *CEAREX Drift Group*, 1990], Arctic Leads Experiment (LEADEX) [e.g., *LEADEX Group*, 1993], the SHEBA project [e.g., *SHEBA Science Working Group*, 1994; *Perovich et al.*, 1999], Beaufort and Arctic Storms Experiment (BASE) [e.g., *Asuma et al.*, 1998], the FIRE First ISCCP (International Satellite Cloud Climatology Project) Regional Experiment [e.g., *Curry et al.*, 2000], the Mixed-Phase Arctic Cloud Experiment (M-PACE) [e.g., *Verlinde et al.*, 2007], etc. However, it is especially difficult to obtain simultaneous long-term observations of Arctic clouds, sea ice and atmospheric convection, especially during polar night. We are interested in such a long-term statistical characterization of the Arctic polar night cloud feedback, and a convenient – though certainly not perfect – starting point could be the use of reanalysis model output.

[9] The purpose of this paper is, therefore, to use reanalysis model output to analyze the relationship between sea ice and clouds in Arctic winter, and to determine whether this relationship is consistent with the mechanism of the convective cloud feedback. In particular, we analyze changes in winter longwave cloud radiative forcing (CRF) associated with anomalies in sea-ice concentration (SIC) over the past three decades to try to deduce the reanalysis models' estimate of the change in cloud radiative forcing that would result from a complete loss of Arctic sea ice.

[10] We emphasize in the strongest terms that reanalysis model output of clouds and surface fluxes in the Arctic are effectively unconstrained by observations. Furthermore, it is well known that reanalysis products suffer large errors in their estimates of energy fluxes (e.g., in shortwave downwelling fluxes which are not directly relevant to our study of a winter-time polar-night feedback, but still indicative of related reanalysis errors [*Serreze et al.*, 1998]). Similarly, comparison with the North Slope of Alaska Barrow site of the Atmospheric Radiation Measurement Program [*Walsh et al.*, 2009] indicates that systematic errors in cloud cover in reanalysis products lead to significant radiation errors as well. To emphasize this point, we refer throughout the paper to "reanalysis model output" rather than "reanalysis products". The present effort cannot, therefore, be seen as an observational test of the convective cloud feedback. Rather, the novelty of the analysis presented here is in testing this feedback in the context of present-day Arctic winter climate variability as opposed to increased greenhouse gas concentration future climate scenarios. The conclusions are only as good as are the two models on which the present analysis is based.

[11] In spite of these caveats, we do feel that the analysis adds an interesting perspective to previous results based on scenarios at high CO_2 and thus advances our understanding of this feedback and its relevance to past, present and future climate change.

2. Reanalysis Model Output and Methods

[12] The two model outputs we use in this study are from the National Center for Environmental Prediction/National Center for Atmospheric Research (NCEP/NCAR) reanalysis [*Kalnay et al.*, 1996] and the European Center for Mid-Range Weather Forecasting (ECMWF) ERA-40 reanalysis (hereinafter ERA-40) [*Uppala et al.*, 2005]. While both products represent model interpolation of data collected by satellites, weather balloons, and surface-based observations, their Arctic output is essentially unconstrained by observations and should therefore be considered model output rather than observations.

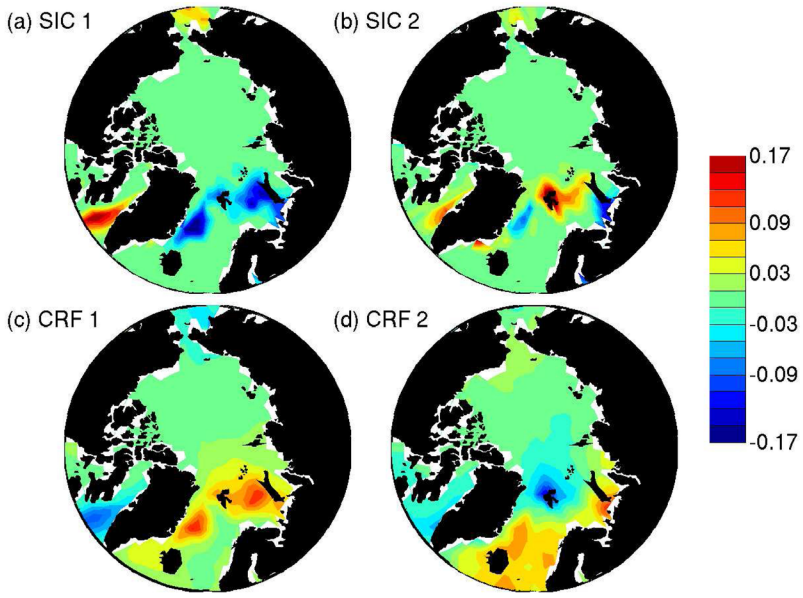

Figure 1. (a, c) First and (b, d) second modes of the singular value decomposition of the covariance matrix of the sea-ice concentration (Figures 1a and 1b) and longwave cloud radiative forcing (Figures 1c and 1d) from the ECMWF ERA-40 model during January and February.

[13] The cloud radiative forcing is a measure of the effect of clouds on radiative balance. It is calculated in the reanalysis as the difference between full-sky radiative flux and clear-sky radiative flux (calculated by rerunning the radiative scheme with the same temperature and moisture profile, but all clouds set to zero). Clouds tend to reflect shortwave (solar) radiation, leading to negative cloud radiative forcing and cooling, although this effect will be minimized during Arctic winter due to low solar flux. Clouds also tend to absorb longwave (terrestrial infrared) radiation, leading to positive cloud radiative forcing and warming. The higher a cloud the lower its emission temperature, and therefore the more longwave cloud radiative forcing it can provide.

[14] Given that the convective cloud feedback should be most active in the winter, we focus on the months of January and February in this paper (henceforth "winter"). We only analyze the area north of 60°N, where shortwave effects of clouds are negligible during winter. CRF refers here to top-of-the-atmosphere values, chosen because the heat balance of an atmospheric column is determined at this level. Every component of the analysis, however, was repeated using surface CRF. Figures and tables related to the surface CRF analysis are provided as well. Cloud radiative forcing is relatively poorly constrained by observational data in the reanalysis products [*Kalnay et al.*, 1996; *Uppala et al.*, 2005], especially in the Arctic. Some satisfaction (even if not any measure of confidence) may be drawn from results that are robust between the two independent reanalysis models.

[15] We identify the dominant modes of coupled SIC and CRF variability using singular value decomposition of their covariance matrix (henceforth SVD analysis) [*Bretherton et al.*, 1992]. SVD analysis of the covariance matrix allows the determination of the most correlated spatial structures between two different time-varying, space-dependent variables. The analysis is useful even when the correlation is not local. That is, variability in one field at one location is correlated with variability at a different location in another field. The analysis involves calculating left and right eigenvectors (also referred to below as SVD modes or SVD pair) of the correlation matrix between SIC and CRF. Let the two dimensional CRF field at a time t be arranged in an $N_{CRF} \times 1$-vector $\mathbf{R}(t)$, and the SIC in a $N_{SIC} \times 1$ vector $\mathbf{I}(t)$, where each element of these vectors is detrended, and then nondimensionalized by removing its mean and dividing it by its standard deviation. Next, define the elements of the $N_{CRF} \times N_{SIC}$ correlation matrix C between the CRF and SIC via an average over the observations given at N_t different times,

Table 1. Fraction of Covariance and Variance Explained by the First Four SVD Modes of the Covariance of SIC and CRF Anomalies From the ECMWF ERA-40 Model, During January and February[a]

SVD	% Covar	% CRF	% SIC	r
1	28	7	29	−0.85
2	11	5	10	−0.54
3	7	4	8	−0.74
4	5	3	6	−0.68

[a]Columns represent: SVD mode number; percent of covariance between SIC and longwave CRF explained by each mode; percent of CRF variance explained; percent of SIC variance explained; the correlation coefficient between CRF and SIC. For all modes shown, the p-value testing against the null hypothesis that SIC and CRF are uncorrelated spatially is less than 0.0001.

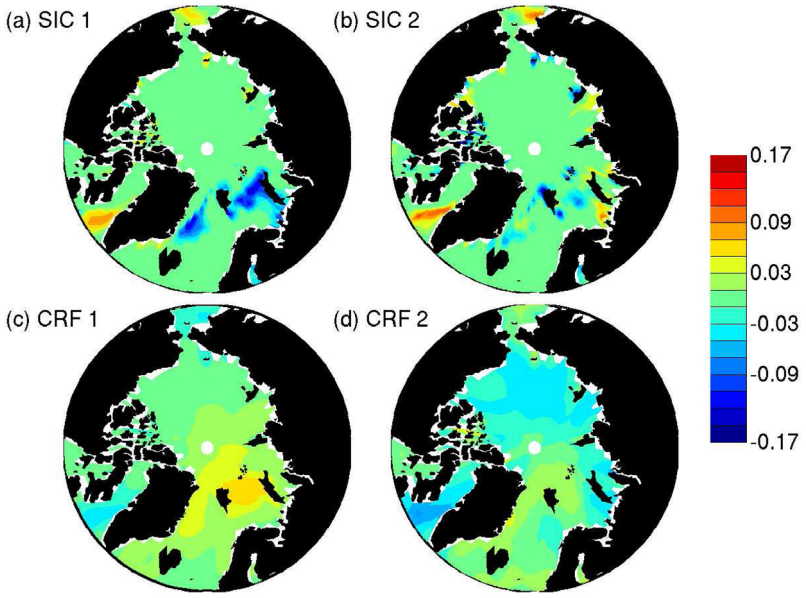

Figure 2. First two SVD modes for SIC and CRF as in Figure 1, but for the NCEP/NCAR model.

$$C_{ij} = \frac{1}{N_t - 1} \sum_{t=1}^{N_t} I_i(t) R_j(t). \quad (1)$$

Here, $I_t(t)$ and $R_j(t)$ are the SIC and CRF at a time t and locations i and j, correspondingly (i and j represent both latitude and longitude and vary over the entire relevant Arctic region). The singular values λ_k and right and left eigenvectors of the covariance matrix C satisfy

$$\mathrm{C}\mathbf{e}^{(R,k)} = \lambda_k \mathbf{e}^{(I,k)}$$

$$\mathrm{C}^T \mathbf{e}^{(I,k)} = \lambda_k \mathbf{e}^{(R,k)},$$

where $\mathbf{e}^{(I,k)}$ is the kth SIC vector and $\mathbf{e}^{(R,k)}$ the kth CRF vector. Writing the singular values λ_k as the diagonal elements of a diagonal matrix Λ and the matrices of the eigenvectors as

$$\mathrm{e}^{(R)} = \left[\mathbf{e}^{(R,1)}, \ldots, \mathbf{e}^{(R,N_{CRF})}\right] \quad (2)$$

$$\mathrm{e}^{(I)} = \left[\mathbf{e}^{(I,1)}, \ldots, \mathbf{e}^{(I,N_{SIC})}\right], \quad (3)$$

the SVD decomposition is

$$\mathrm{C} = \left(\mathrm{e}^{(I)}\right)^T \Lambda \mathrm{e}^{(R)}. \quad (4)$$

The right and left eigenvectors corresponding to the largest eigenvalues represent the spatial patterns accounting for the largest fraction of the covariance between the two fields. For example, if the first pair of SVD vectors (corresponding to the largest eigenvalue λ_1) shows a region with both lower-than-average sea ice and higher-than-average cloud radiative forcing, this indicates that these phenomena often occur simultaneously in the time series. If the convective cloud feedback hypothesis, a local effect, is correct, one would expect a strong anti-correlation in space between SIC and CRF SVD vectors (that is, similar yet opposite-signed spatial anomaly patterns in the SIC and CRF fields of a given SVD pair). A positive correlation would imply CRF increased when and where SIC increased, which is clearly inconsistent with the hypothesis. No correlation would imply that changes in CRF were unrelated to changes in SIC, which would also be inconsistent with the hypothesis. We perform this analysis on the anomalies of SIC and CRF from the mean for each day during winter, with trends over the analysis period removed from the time series of both variables.

[16] In order to characterize the strength of the correlation between SIC and CRF, we first calculate the line of best fit between the daily SIC anomalies and CRF anomalies during winter at each grid point. We then extrapolate this line of best fit to 100% SIC loss at each grid point in order to obtain a crude estimate of the increase in CRF that would be associated with a complete loss of sea ice at that point. We only use this metric

Table 2. Fraction of Covariance as in Table 1, but for the NCEP/NCAR Model[a]

SVD	% Covar	% CRF	% SIC	r
1	16	11	13	−0.52
2	8	5	22	−0.37
3	7	4	28	−0.39
4	5	2	36	−0.45

[a]For all modes shown the p-value testing against the null hypothesis that SIC and CRF are uncorrelated spatially is less than 0.0001.

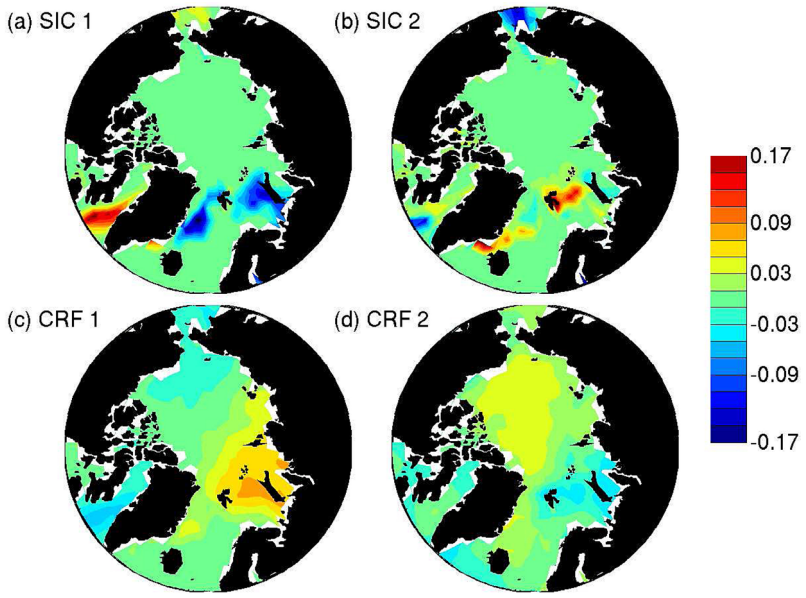

Figure 3. First two SVD modes of SIC and CRF as in Figure 1 (ECMWF ERA-40), but for surface CRF rather than top-of-the-atmosphere. Anticorrelation is apparent but is visually weaker and less localized than for top-of-the-atmosphere CRF.

when the p-value testing against the null hypothesis that sea-ice concentration and longwave cloud radiative forcing are unrelated is less than 0.05 and the standard deviation of sea-ice concentration (fraction) variation is greater than 0.05. These tests identify regions where observed variability is nearly between completely ice-free and completely ice-covered, which makes this a minimal extrapolation. We note that this extrapolation still adds some uncertainty to the interpretation. We use this extrapolated estimate as a measure of the strength of the relationship between SIC anomalies and CRF anomalies. This strength, in turn, can be used to gauge the consistency of the reanalysis model output with the convective cloud feedback in other models and suggest what strength the feedback would have if active. Note that the feedback involves the response of CRF to SIC loss, and vice versa. Although our methodology does not allow us to determine causality, it does allow us to establish the strength of the relationship. Finally, in order to test for statistical significance of the results we calculate a p-value. We account for temporal auto-correlation using the phase-randomization approach of

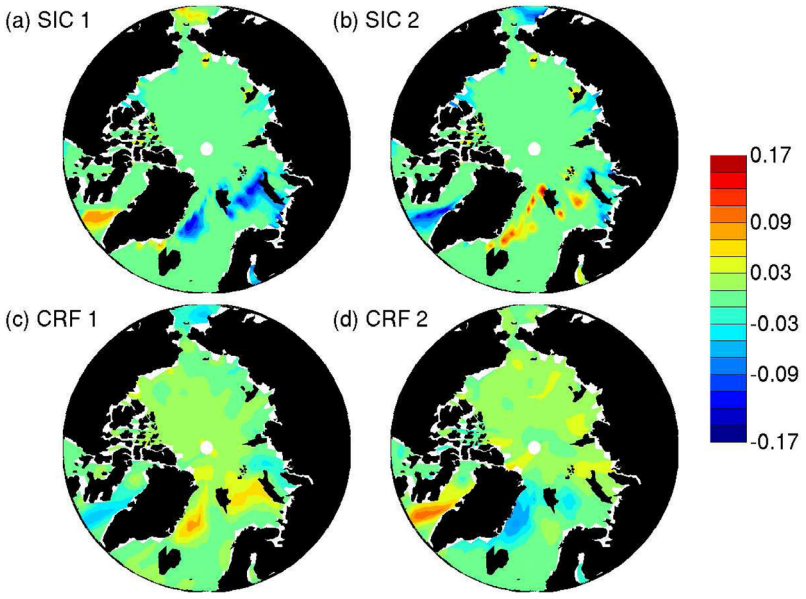

Figure 4. First two SVD modes as in Figure 2 (NCEP/NCAR), but for surface CRF rather than top of the atmosphere. Anti-correlation is apparent with similar strength and localization as for top-of-the-atmosphere CRF.

Stine et al. [2009], based on the null hypothesis that SIC and CRF are unrelated and only include points for which the p-value is less than 0.05. We also treat points for which the standard deviation of SIC is less than 0.05 as insignificant for the purpose of estimating the strength of the feedback.

3. Results

[17] Figure 1 contains the first two modes of the SVD analysis of the covariance matrix between SIC and CRF for the ERA-40 model output and Table 1 contains statistics on the first four SVD modes. Figure 2 and Table 2 contain the corresponding modes for the NCEP/NCAR model output. The most striking feature of the SVD modes is the strong spatial anti-correlation between SIC and CRF that they exhibit. For example, all of the first 20 SVD modes of ERA-40, which together explain 85% of the SIC and CRF covariation in that model, and all of the first 20 SVD modes of the NCEP/NCAR model output, which together explain 64% of the SIC and CRF covariation in that model, are significantly anti-correlated at a p-value of 0.0001. This indicates that the covariation between SIC and CRF is primarily driven locally, rather than remotely. The SIC anomaly pattern in the first mode in both models resembles the SIC anomaly pattern produced by the North Atlantic Oscillation [*Deser and Teng*, 2008], but the identification of the modes of covariation with named modes of variation is less important for our purposes than the strong anti-correlation between SIC and CRF. Figures 3 and 4, along with Tables 3 and 4, contain the results of the SVD analysis using surface CRF; in general they are similar to the results of the top-of-the-atmosphere analysis and lead to similar conclusions.

[18] Figure 5 shows a map of the strength of the relationship between SIC and CRF anomalies (as defined in section 2) in the ERA-40 and NCEP/NCAR models. The regions where this relationship is significant are located on the fringe of winter sea-ice extent, where the largest fluctuations in SIC from seasonal climatology occur. Our methodology produces an estimate for the CRF increase associated with a complete local removal of sea ice of ~10–25 W m^{-2} in the NCEP/NCAR model and ~15–30 W m^{-2} in the ERA-40 model. Figure 6 is an analogous strength map using surface CRF, which is again very similar.

[19] So far we have demonstrated a link between both top-of-the-atmosphere and surface CRF on the one hand, and sea ice on the other. Of course, CRF may increase even with no change to convection or clouds, simply due to an increase in surface temperature (due to opening of leads, for example) and the resulting increase in outgoing longwave radiation. In order to demonstrate that convection is indeed involved in this link, we therefore consider an SVD analysis of convective precipitation and sea-ice concentration for both reanalyses (Figures 7 and 8). The sea ice and convective precipitation variability patterns are again clearly correlated locally, consistent with the possibility that convection may be the link between SIC and CRF. Tables 5 and 6 reinforce this impression and show the local anti-correlation between sea ice and convective precipitation to be highly significant. As discussed below, these results cannot be taken as a proof that the convective cloud feedback is involved, but they seem to strongly suggest that this may be the case.

Table 3. Fraction of Covariance and Variance Explained by the First Four SVD Modes of the Covariance of SIC and Surface CRF Anomalies From the ECMWF ERA-40 Model, During January and February[a]

SVD	% Covar	% CRF	% SIC	r
1	25	12	27	−0.46
2	9	14	7	−0.23
3	7	6	8	−0.17
4	5	2	5	−0.32

[a]Columns represent: SVD mode number; percent of covariance between SIC and surface longwave CRF explained by each mode; percent of surface CRF variance explained; percent of SIC variance explained; the correlation coefficient between surface CRF and SIC. For all modes shown, the p-value testing against the null hypothesis that SIC and surface CRF are uncorrelated spatially is less than 0.0001. Anti-correlation is generally lower than for top-of-the-atmosphere CRF but is still very pronounced.

4. Discussion

[20] The strong local relationship found here in two models between the covariation of sea ice (SIC) and cloud radiative forcing (CRF) fields, is consistent with the convective-cloud feedback being active in their simulation of present-day Arctic variability. This local feedback may therefore contribute significantly to the variability and covariation of SIC and CRF in these two models. Furthermore, we find that the increases in CRF associated with decreases in SIC are accompanied by increases in convective precipitation rate. Since convective precipitation rate is the variable most closely associated with convection in the NCEP/NCAR and ERA-40 model output, we interpret this as suggesting that convection may be the link between SIC and CRF. In this scenario, when sea ice recedes as part of the seasonal or interannual variability, convection turns on and CRF increases; although other processes cannot be ruled out based on these results alone, both model outputs are consistent with the convective cloud feedback and suggest that it may be contributing to the covariation between SIC and CRF during winter. However, the

Table 4. Fraction of Covariance of SIC and Surface CRF, as in Table 3, but for the NCEP/NCAR Model[a]

SVD	% Covar	% CRF	% SIC	r
1	11	8	12	−0.44
2	7	5	6	−0.37
3	5	3	11	−0.20
4	5	3	6	−0.28

[a]For all modes shown the p-value testing against the null hypothesis that SIC and surface CRF are uncorrelated spatially is less than 0.0001. Anti-correlation is generally slightly lower than for top-of-the-atmosphere CRF but is still very pronounced.

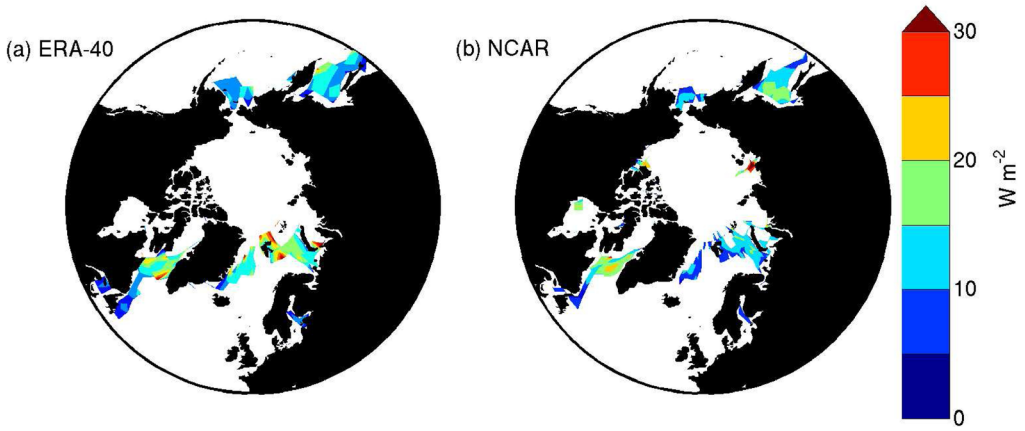

Figure 5. Estimated increase in January and February longwave cloud radiative forcing associated with the complete removal of sea ice in the (a) ECMWF ERA-40 and (b) NCEP/NCAR models. Estimates are only plotted when the p-value testing against the null hypothesis that sea-ice concentration and longwave cloud radiative forcing are unrelated is less than 0.05 and the standard deviation of sea-ice concentration (fraction) variation is greater than 0.05.

statistical analysis here cannot prove the relationship between SIC and CRF is causal.

[21] The convective cloud feedback requires some external forcing to be initiated. One possible forcing, which may be relevant to both past and future climates, is increased greenhouse gas levels [*Abbot and Tziperman*, 2008b]. For the anomalies in ice cover analyzed here the forcing is likely changes in atmospheric and ocean heat transport, as well as the movement of sea ice forced by atmospheric dynamics. For example, the first SIC mode resembles the pattern expected from the North Atlantic oscillation (section 3). Finally, while we have attempted to characterize the strength of the relationship between SIC and CRF, it is possible that an external factor such as mentioned above participates in the initiation of the sea-ice anomalies, while the feedback may enhance them. A complete feedback loop implies that SIC anomalies would lead to CRF changes and those increase the initial SIC anomalies. The uncertainty regarding the role of some external third factor implies that our analysis does not prove the existence of such a complete feedback loop between sea ice and convective clouds and only indicates that their variability is consistent with such a feedback.

[22] The model evidence of present-day variability we analyze here indicates that complete loss of wintertime sea ice at a given grid point corresponds to a CRF increase of ~10–30 W m^{-2}. Yet there are several important questions left open, not allowing this to be considered a verification of the existence of a convective cloud feedback. First, CRF may increase merely because surface temperature does, even with fixed clouds. It is not possible to pull out the effect of increased temperature on CRF in our analysis, even if we do show enhanced convective precipitation which suggests that convective clouds do increase during negative SIC anomalies. Second, it is not possible to establish using our methodology whether the CRF increase is due primarily to increased cloud fraction or cloud optical thickness. Third, the increase in both atmospheric

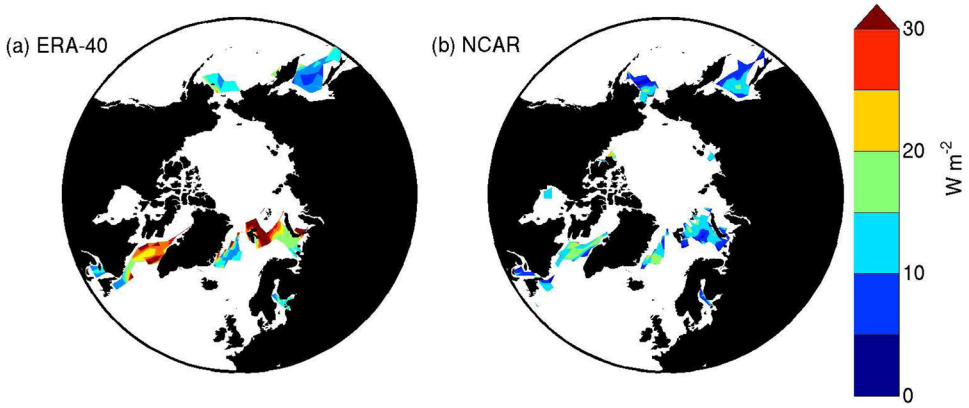

Figure 6. Estimated strength of SIC-CRF correlation as in Figure 5, but for surface CRF. (a) For ERA-40 the increase in surface CRF associated with complete removal of sea ice is noticeably greater than the increase in top-of-the-atmosphere CRF in some areas. (b) For NCEP/NCAR the difference is less pronounced.

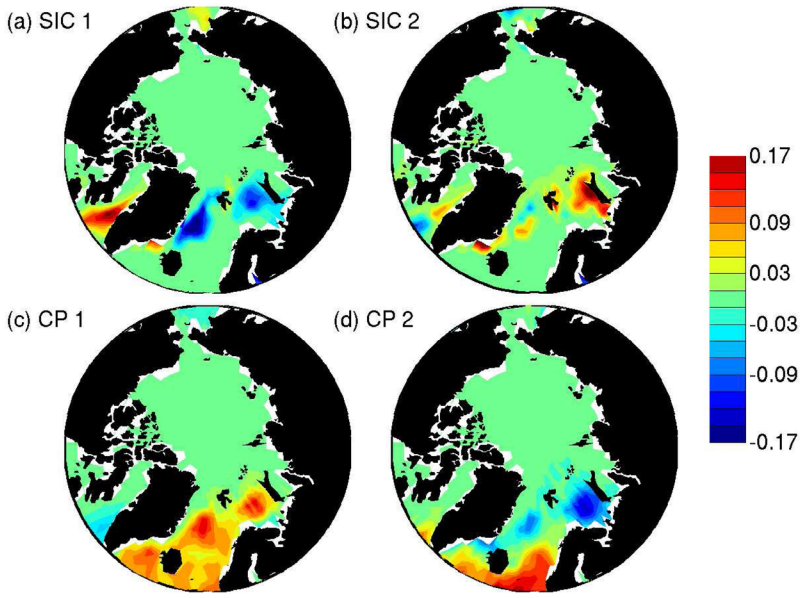

Figure 7. (a, c) First and (b, d) second modes of the singular value decomposition of the covariance matrix of sea-ice concentration (Figures 7a and 7b) and the logarithm of the convective precipitation rate (Figures 7c and 7d) from the ECMWF ERA-40 model during January and February. The logarithm of the convective precipitation rate was taken to properly handle near-zero values at extreme northern latitudes and because the response of convective precipitation to sea-ice concentration is of greater interest than actual convective precipitation values. Localized anti-correlation is visually apparent.

temperature and in evaporation and therefore atmospheric water vapor, in areas of reduced sea ice, will also lead to enhanced downwelling LW radiation, and some of the sea ice decrease may be attributed to these effects rather than to the CRF of convective clouds.

[23] In spite of these uncertainties, it is interesting to note that the IPCC models in which the convective cloud feedback is most active (NCAR's CCSM and MPI's MPI-ECHAM [see *Abbot et al.*, 2009b]) the CRF increases by ~25 W m^{-2} in the deep Arctic and 10–25 W m^{-2} in sub-Arctic upon the complete removal of winter sea ice [*Abbot et al.*, 2009b], and that the CRF is calculated consistently in these models as with the reanalysis (including the same limitations). In those

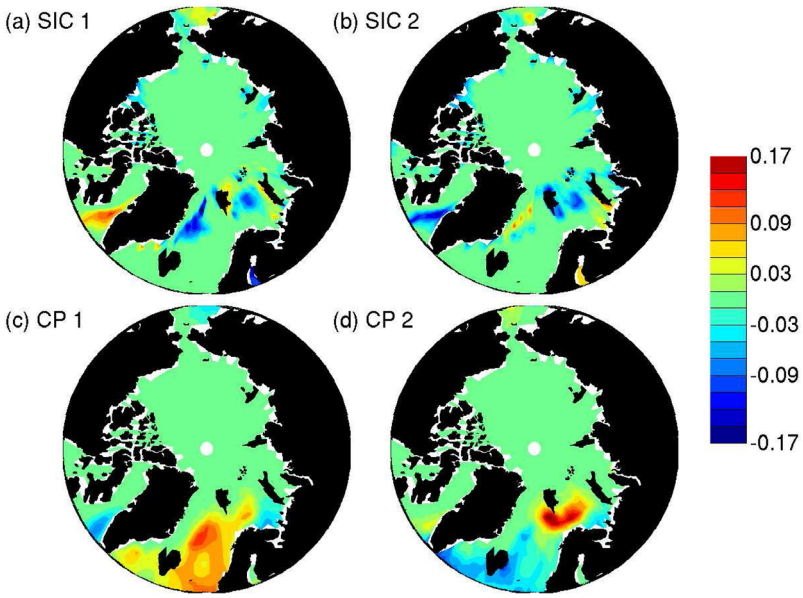

Figure 8. First two SVD modes for convective precipitation and sea ice as in Figure 7, but for NCEP/NCAR. Localized anticorrelation is visually apparent, although less so than for ECMWF ERA-40. As was the case in the analysis of CRF, the ERA-40 model shows stronger anti-correlation than NCEP/NCAR.

Table 5. Fraction of Covariance and Variance Explained by the First Four SVD Modes of the Covariance of SIC Anomalies and the Logarithm of Convective Precipitation Rate From the ECMWF ERA-40 Model, During January and February[a]

SVD	% Covar	% CP	% SIC	r
1	23	10	24	−0.41
2	10	8	10	−0.38
3	8	4	10	−0.36
4	5	5	5	−0.25

[a]Columns represent: SVD mode number; percent of covariance between SIC and convective precipitation rate explained by each mode; percent of convective precipitation rate variance explained; percent of SIC variance explained; the correlation coefficient between convective precipitation rate and SIC. For all modes shown, the p-value testing against the null hypothesis that SIC and convective precipitation rate are uncorrelated spatially is less than 0.0001. Results indicate that SIC and convective precipitation rate are strongly and locally anticorrelated.

two models it was possible to show explicitly that winter sea ice is eliminated from the entire Arctic by a combination of the convective cloud feedback and an ocean heat transport feedback when CO_2 is quadrupled. The agreement between the CRF response to sea-ice loss of the reanalysis models and those two IPCC models suggests that complete loss of winter sea ice at quadrupled CO_2 may be more likely than is implied by the fact that only two of the IPCC models have completely lost winter sea ice at this CO_2 concentration.

[24] We reemphasize, of course, that reanalysis model output used here is effectively unconstrained by observations in the Arctic so that this is by no means an observational verification. Additionally, it is interesting to note that the NCAR and MPI models are the IPCC models that produce the best simulation to date of the warm, equable, sea-ice free climates of the early Eocene (~56 to ~34 million years ago) and that the convective cloud feedback is active in these simulations [*Huber*, 2009; *Abbot et al.*, 2009a; *Heinemann et al.*, 2009].

[25] There is some disagreement between the ERA-40 and NCEP/NCAR model results. For example, both the strength of the SIC-CRF relationship (Figure 5) and the spatial anti-correlation in the modes of SIC and CRF covariation (Tables 1 and 2) are generally higher in the ERA-40 model than in the NCEP/NCAR model. This underscores the fact that the results presented here are based on uncertain model output. Analysis of in-situ and remote sensing data, rather than reanalysis models, must be performed before firmer conclusions can be drawn. Additionally, a proper comparison between models and data would require the calculation of the exact same statistics in model runs during the modern era as in observational record. Nevertheless, we feel that the analysis we have performed here is a significant first step in the effort to determine whether the convective cloud feedback may be a major player in wintertime Arctic sea-ice variability and changes. It is interesting that despite differences between the two models analyzed here, both show a relationship between SIC and CRF anomalies consistent with a convective cloud feedback that is as strong as that produced in the IPCC models that produce the strongest convective cloud feedback.

Table 6. Fraction of Covariance and Variance of SIC and Convective Precipitation as in Table 5, but for the NCEP/NCAR Model[a]

SVD	% Covar	% CP	% SIC	r
1	12	16	7	−0.16
2	8	7	7	−0.16
3	7	4	11	−0.26
4	6	4	7	−0.23

[a]For all modes shown, the p-value testing against the null hypothesis that SIC and convective precipitation rate are uncorrelated spatially is less than 0.0001. Results indicate that SIC and convective precipitation rate are strongly and locally anticorrelated. The anti-correlation is weaker than for ECMWF ERA-40, but is still apparent.

[26] **Acknowledgments.** We thank Chris Walker for technical assistance, Peter Huybers for advice on statistics, and the editors and anonymous reviewers for the Journal of Advances in Modeling Earth Systems, the Journal of Climate and Geophysics Research Letters, for their constructive and helpful comments and for their patience while we slowly learned the limitations of Arctic reanalysis products. This work was supported by the NSF P2C2 program (ATM-0902844). DSA was supported by the T. C. Chamberlin Fellowship of the University of Chicago and the Canadian Institute for Advanced Research. ET thanks the Weizmann Institute for its hospitality during parts of this work.

References

Abbot, D. S., and E. Tziperman (2008a), A high latitude convective cloud feedback and equable climates, *Q. J. R. Meteorol. Soc.*, *134*, 165–185, doi:10.1002/qj.211.

Abbot, D. S., and E. Tziperman (2008b), Sea ice, high-latitude convection, and equable climates, *Geophys. Res. Lett.*, *35*, L03702, doi:10.1029/2007GL032286.

Abbot, D. S., M. Huber, G. Bousquet, and C. C. Walker (2009a), High-CO_2 cloud radiative forcing feedback over both land and ocean in a global climate model, *Geophys. Res. Lett.*, *36*, L05702, doi:10.1029/2008GL036703.

Abbot, D. S., C. Walker, and E. Tziperman (2009b), Can a convective cloud feedback help to eliminate winter sea ice at high CO_2 concentrations?, *J. Clim.*, *22*(21), 5719–5731, doi:10.1175/2009JCLI2854.1.

Asuma, Y., S. Iwata, K. Kikuchi, G. Moore, R. Kimura, and K. Tsuboki (1998), Precipitation features observed by doppler radar at Tuktoyaktuk, Northwest Territories, Canada, during the Beaufort and Arctic storms experiment, *Mon. Weather Rev.*, *126*(9), 2384–2405, doi:10.1175/1520-0493(1998)126<2384:PFOBDR>2.0.CO;2.

Bretherton, C. S., C. Smith, and J. M. Wallace (1992), An intercomparison of methods for finding coupled patterns in climate data, *J. Clim.*, *5*(6), 541–560, doi:10.1175/1520-0442(1992)005<0541:AIOMFF>2.0.CO;2.

Brummer, B. (1997), Boundary layer mass, water, and heat budgets in wintertime cold-air outbreaks from the Arctic sea ice, *Mon. Weather Rev.*, *125*(8), 1824–1837, doi:10.1175/1520-0493(1997)125<1824:BLMWAH>2.0.CO;2

CEAREX Drift Group (1990), CEAREX Drift Experiment, *Eos Trans. AGU*, *71*(40), 1115.

Curry, J., P. Hobbs, M. King, D. Randall, and P. Minnis (2000), FIRE Arctic clouds experiment, *Bull. Am. Meteorol. Soc.*, *81*(1), 5–29, doi:10.1175/1520-0477(2000)081<0005:FACE>2.3.CO;2.

Curry, J. A., and E. E. Ebert (1992), Annual cycle of radiation fluxes over the Arctic Ocean: Sensitivity to cloud optical properties, *J. Clim.*, *5*, 1267–1280, doi:10.1175/1520-0442(1992)005<1267:ACORFO>2.0.CO;2.

Deser, C., and H. Teng (2008), Evolution of Arctic sea ice concentration trends and the role of atmospheric circulation forcing, 1979–2007, *Geophys. Res. Lett.*, *35*, L02504, doi:10.1029/2007GL032023.

Heinemann, M., J. Jungclaus, and J. Marotzke (2009), Warm Paleocene/Eocene climate as simulated in ECHAM5/MPI-OM, *Clim. Past*, *5*(4), 785–802, doi:10.5194/cp-5-785-2009.

Huber, M. (2009), Snakes tell a torrid tale, *Nature*, *457*(7230), 669–671, doi:10.1038/457669a.

Kalnay, E., et al. (1996), The NCEP/NCAR 40-year reanalysis project, *Bull. Am. Meteorol. Soc.*, *77*, 437–471, doi:10.1175/1520-0477(1996)077<0437:TNYRP>2.0.CO;2.

Kay, J. E., and A. Gettelman (2009), Cloud influence on and response to seasonal Arctic sea ice loss, *J. Geophys. Res.*, *114*, D18204, doi:10.1029/2009JD011773.

LEADEX Group (1993), The LEADEX experiment, *Eos Trans. AGU*, *74*, 393–397.

Liu, Y., J. R. Key, and X. Wang (2008), The influence of changes in cloud cover on recent surface temperature trends in the Arctic, *J. Clim.*, *21*(4), 705–715, doi:10.1175/2007JCLI1681.1.

McBean, G., et al. (2005), Arctic climate: Past and present, in *Arctic Climate Impact Assessment*, edited by C. Symon, L. Arris, and B. Heal, pp. 22–60, Cambridge Univ. Press, Cambridge, U. K.

Palm, S. P., S. T. Strey, J. Spinhirne, and T. Markus (2010), Influence of Arctic sea ice extent on polar cloud fraction and vertical structure and implications for regional climate, *J. Geophys. Res.*, *115*, D21209, doi:10.1029/2010JD013900.

Perovich, D. K., et al. (1999), Year on ice gives climate insights, *Eos Trans. AGU*, *80*(41), 481, doi:10.1029/EO080i041p00481-01.

Pinto, J. O., J. A. Curry, and K. L. McInnes (1995), Atmospheric convective plumes emanating from leads: 1. Thermodynamic structure, *J. Geophys. Res.*, *100*(C3), 4621–4631, doi:10.1029/94JC02654.

Schnell, R. C., R. G. Barry, M. W. Miles, E. L. Andreas, L. F. Radke, C. A. Brock, M. P. McCormick, and J. L. Moore (1989), Lidar detection of leads in Arctic sea ice, *Nature*, *339*, 530–532, doi:10.1038/339530a0.

Schweiger, A. J., R. W. Lindsay, S. Vavrus, and J. A. Francis (2008), Relationships between Arctic sea ice and clouds during autumn, *J. Clim.*, *21*(18), 4799–4810, doi:10.1175/2008JCLI2156.1.

Serreze, M., J. Key, J. Box, J. Maslanik, and K. Steffen (1998), A new monthly climatology of global radiation for the Arctic and comparisons with NCEP-NCAR reanalysis and ISCCP-C2 fields, *J. Clim.*, *11*(2), 121–136, doi:10.1175/1520-0442(1998)011<0121:ANMCOG>2.0.CO;2.

SHEBA Science Working Group (1994), New program to research issues of global climate in the Arctic, *Eos Trans. AGU*, *75*(22), 249.

Shupe, M., and J. Intrieri (2004), Cloud radiative forcing of the Arctic surface: The influence of cloud properties, surface albedo, and solar zenith angle, *J. Clim.*, *17*(3), 616–628, doi:10.1175/1520-0442(2004)017<0616:CRFOTA>2.0.CO;2.

Smetacek, V., and S. Nicol (2005), Polar ocean ecosystems in a changing world, *Nature*, *437*(7057), 362–368, doi:10.1038/nature04161.

Stine, A. R., P. Huybers, and I. Y. Fung (2009), Changes in the phase of the annual cycle of surface temperature, *Nature*, *457*(7228), 435–440, doi:10.1038/nature07675.

Uppala, S. M., et al. (2005), The ERA-40 re-analysis, *Q. J. R. Meteorol. Soc.*, *131*(612), 2961–3012, doi:10.1256/qj.04.176.

Verlinde, J., et al. (2007), The mixed-phase Arctic cloud experiment, *Bull. Am. Meteorol. Soc.*, *88*(2), 205+, doi:10.1175/BAMS-88-2-205.

Walsh, J. E., W. L. Chapman, and D. H. Portis (2009), Arctic cloud fraction and radiative fluxes in atmospheric reanalyses, *J. Clim.*, *22*(9), 2316–2334, doi:10.1175/2008JCLI2213.1.

Walter, B. (1980), Wintertime observations of roll clouds over the Bering Sea, *Mon. Weather Rev.*, *108*(12), 2024–2031, doi:10.1175/1520-0493(1980)108<2024:WOORCO>2.0.CO;2.

Winton, M. (2006), Does the Arctic sea ice have a tipping point?, *Geophys. Res. Lett.*, *33*, L23504, doi:10.1029/2006GL028017.

Zulauf, M. A., and S. K. Krueger (2003a), Two-dimensional cloud-resolving modeling of the atmospheric effects of Arctic leads based upon midwinter conditions at the Surface Heat Budget of the Arctic Ocean ice camp, *J. Geophys. Res.*, *108*(D10), 4312,, doi:10.1029/2002JD002643.

Zulauf, M. A., and S. K. Krueger (2003b), Two-dimensional numerical simulations of Arctic leads: Plume penetration height, *J. Geophys. Res.*, *108*(C2), 8050, doi:10.1029/2000JC000495.

Corresponding author: E. Tziperman, Department of Earth and Planetary Sciences, Harvard University, 20 Oxford St., Cambridge, MA 02138, USA. (eli@eps.harvard.edu)